Evaluation Of a New Reconstruction Technique for Dual-Energy (DECT) Lung Perfusion: Preliminary Experience In 58 Patients

J. Pinilo, Antoine Hutt, Julien Labreuche, Jean-Baptiste Faivre, T. Flohr, B. Schmidt, Alain Duhamel, Jacques Remy, Martine Remy

Version of Record: https://www.sciencedirect.com/science/article/pii/S107663322100338X
Manuscript_9f8a3ad6df0057d0a3ca8ea1e29051d2

EVALUATION OF A NEW RECONSTRUCTION TECHNIQUE FOR DUAL-ENERGY (DECT) LUNG PERFUSION: PRELIMINARY EXPERIENCE IN 58 PATIENTS

Authors:

Juliette Pinilo, MD[1]

Antoine Hutt, MD[1]

Julien Labreuche, PhD[2]

Jean-Baptiste Faivre, MD[1]

Thomas Flohr, PhD[3]

Bernhard Schmidt, PhD[3]

Alain Duhamel, PhD[2]

Jacques Remy, MD[1]

Martine Remy-Jardin, MD, PhD[1]

Authors' affiliations and addresses:

[1]Univ.Lille, CHU Lille, Department of Thoracic Imaging, ULR 2694 METRICS Evaluation des technologies de santé et des pratiques médicales, F-59000 LILLE, France
Hospital Calmette, University Hospital Center of Lille, Blvd Jules Leclercq F-59000 LILLE, France

[2]Univ.Lille, CHU Lille, Department of Biostatistics, ULR 2694 METRICS Evaluation des technologies de santé et des pratiques médicales, F-59000 LILLE, France

[3]Department of CT Research & Development; Siemens Healthcare GmbH, D-91301 Forchheim, Germany

Corresponding author:

Martine REMY-JARDIN, Department of Thoracic Imaging, Hospital Calmette, University Hospital Center of Lille, Blvd Jules Leclercq F-59000 LILLE, France

Phone: 33 3- 20-44-43-11 Fax: 33 3- 20-44-47-20

e-mail address: martine.remy@chru-lille.fr

EVALUATION OF A NEW RECONSTRUCTION TECHNIQUE FOR DUAL-ENERGY (DECT) LUNG PERFUSION: PRELIMINARY EXPERIENCE IN 58 PATIENTS

ABSTRACT

Purpose: To compare dual-energy (DE) lung perfused blood volume generated by subtraction of virtual monoenergetic images (Lung Mono) with images obtained by three-compartment decomposition (Lung PBV).

Material and methods:

The study included 58 patients (28 patients with and 30 patients without PE) with reconstruction of Lung PBV images (i.e., the reference standard) and Lung Mono images. The inter-technique comparison was undertaken at a patient and segment level.

Results: The distribution of scores of subjective image noise (patient level) significantly differed between the two reconstructions ($p<0.0001$), with mild noise in 58.6% (34/58) of Lung Mono images vs 25.9% (15/58) of Lung PBV images. Detection of perfusion defects (segment level) was concordant in 1104 segments (no defect: n=968; defects present: n=138) and discordant in 2 segments with a PE-related defect only depicted on Lung Mono images. Among the 28 PE patients, the distribution of gradient of attenuation between perfused areas and defects was significantly higher on Lung Mono images compared to Lung PBV (median= 73.5 HU (QI=65.0; Q3=86.0) vs 24.5 HU (22.0; 30.0); $p<0.0001$). In all patients, fissures were precisely identified in 77.6% of patients (45/58) on Lung Mono images while blurred (30/58; 51.7%) or not detectable (28/58; 48.3%) on Lung PBV images.

Conclusion: Lung Mono perfusion imaging allows significant improvement in the overall image quality and improved detectability of PE-type perfusion defects.

KEY WORDS: dual-energy CT; lung perfusion; monoenergetic imaging; actue pulmonary embolism; pulmonary arteries

ABBREVIATIONS: DE: dual energy; DECT: dual-energy compouted tomography; PBV: pulmonary blood volume; Mono+: monoenergetic plus; keV: kilo-electronvolt

INTRODUCTION

Dual-energy CT (DECT), also called spectral or multi-energy CT, has gained wide acceptance in clinical practice owing to its unique post-processing capabilities enabling optimization of morphologic imaging and introduction of functional imaging. This is accomplished by an almost simultaneous acquisition of datasets with two x-ray beams of different energy, or by using spectral detectors, and then processing the data. Among the most important DECT reconstructions are virtual monoenergetic images, virtual unenhanced images, virtual noncalcium images and iodine maps for perfusion imaging (**1**). In the context of chest imaging, the most frequent clinical objective of DECT angiographic examinations is to provide simultaneous assessment of the pulmonary vasculature and analysis of the parenchymal iodine distribution, both generated from the same data set at a radiation dose similar or moderately higher than single-energy CT pulmonary angiography (**2-7**). The pattern of iodine enhancement has been shown to correspond to lung blood volume at planar scintigraphy and single photon-emission CT (**8,9**) and is considered a surrogate marker of lung perfusion (**10,11**).

In the field of pulmonary vascular diseases, detection of perfusion alterations can help in the diagnostic approach of acute (**12,13**) and chronic (**14-16**) pulmonary embolism but also in the diagnostic work-up of pulmonary hypertension (**17-21**). Numerous additional applications have also been reported in smoking-related diseases (**22,23**), interstitial lung diseases (**24**) and to predict post-operative lung function (**25**) while lung microvascular disease can also be imaged in COVID-19 using DECT lung perfusion imaging (**26-29**).

The technique for assessing pulmonary perfusion on DECT angiographic examinations is based on material decomposition into iodine and soft tissue of different density (mixtures of air and soft tissue). The iodine map visualizes the regional pulmonary distribution of intravenous contrast in distal pulmonary vessels including the capillaries (**30**). Whereas the iodine distribution is interpretable in the majority of cases, there is a well-known influence of patient body habitus on the overall image quality.

Image noise increases with the patient BMI and noise texture gets grainy, coarse and patchy. If image graininess is not a limiting factor for detection of PE-type defects, it may preclude confident depiction of patchy perfusion defects. Furthermore, spatial resolution is reduced in the Lung PBV images, potentially limiting the depiction of small perfusion defects. As an alternative to the established Lung PBV algorithm, dual-energy images of the lungs can also be processed by subtracting virtual monoenergetic images of different energy levels. This approach takes advantage of the improved iodine, contrast-to-noise ratio (CNR) of virtual monoenergetic images, in particular at low energy levels, while maintaining spatial resolution and fine noise texture. To avoid noise increase at lower calculated energies, which is a known drawback of virtual monoenergetic images at low kilo-electron volt (keV), a regional spatial frequency-based combination of the high contrast at lower energies and the superior noise properties at medium energies can be performed to optimize CNR (**31**). These images are called Monoenergetic Plus (i.e., Mono+).

The purpose of our study was to compare the image quality of iodine maps generated by subtraction of virtual Mono+ images with that of the traditional Lung PBV approach. This comparative study was undertaken in the clinical context of acute pulmonary embolism with a primary objective focusing on the detectability of PE-related perfusion defects. The secondary objective was to investigate whether the theoretical improvement in image quality of subtracted mono+ images could be verified in conditions of daily clinical practice.

MATERIAL & METHODS

1-Technical background

The DE Lung Mono prototype (eXamine Version XYZ) subtracts Mono+ images of different energy levels. To visualize iodine distribution, 190 keV Mono+ images are subtracted from 40 keV Mono+ images. The 40 keV images have a highly increased iodine signal on top of the underlaying lung density. The 190 keV images only contains

the lung density information, with practically no iodine signal because of the high keV. The subtraction images therefore show just the increased iodine signal.

In order to assess objectively the differences in noise and spatial resolution between images being processed with the Lung PBV and the DE Lung Mono approach, we used the resolution insert CTP528 of the CAT phantom (Catphan 500, The Phantom Laboratory,USA). Beside homogeneous areas which allow for noise measurements in terms of standard deviation, the phantom contains inserts of line pairs from 1 up to 21 per cm for high resolution measurements. The phantom was scanned in dual-energy mode on a SOMATOM Force (Siemens Healthineers; Forchheim; Germany) with the acquisition parameters listed in **Table 1** and was reconstructed with the default settings (kernel Qr40; FOV 300). Low- and high-energy images were processed with both algorithms, DE Lung PBV and DE Lung Mono. Noise in terms of standard deviation was 11.2 HU and 19.4 HU for the Lung PBV and the Lung Mono, respectively. Despite lower noise in terms of standard deviation, the noise texture was more patchy and grainy for the Lung PBV images. Resolution was maintained in the case of Lung Mono (6 lp/cm), and lower in the case of Lung PBV (4 lp/cm) (**Figure 1**).

2-Study population

From our CT data base prospectively established, we retrospectively selected patients fulfilling the following criteria: (a) a positive or negative dual-energy CT (DECT) angiogram indicated for clinical suspicion of acute PE; (b) positive CT angiograms for PE with at least one defect on perfusion imaging; (c) absence of co-morbid respiratory disease, potentially responsible for perfusion alterations; (d) DECT angiograms obtained on the same CT equipment (i.e., a 3rd generation dual-source CT system; SOMATOM Force; Siemens Healthineers; Forchheim; Germany). All patients referred for clinical suspicion of acute PE who had been scanned with single-energy CT were excluded from the study population. The scanning protocols and reconstruction parameters are summarized in **Table 1**.

We planned to include 30 patients with acute PE and 30 patients without acute PE. Positive PE examinations with perfusion defects were used to select PE-type perfusion defects for comparative analysis on Lung Mono and Lung PBV images; negative PE examinations, subsequently without PE-type defects on Lung PBV, were necessary to ensure the absence of false-positive findings on Lung Mono images.

Patient selection was obtained as follows: (a) between July 2015 (date of installation of the 3-rd generation DSCT scanner in our department) and December 2019 (date of our investigation), 28 consecutive patients with acute PE were eligible (Group 1), including 26 patients with both lungs analyzable and 2 patients with a single lung analyzable owing to the presence of a contralateral lung tumor; (b) in our data base, the first 30 consecutive patients with a negative DECT angiogram for acute PE were selected (Group 2); all patients had been scanned in 2019 and both lungs were analyzable. The limited number of PE-positive patients fulfilling the inclusion criteria is linked to the scanning protocols proposed to patients suspected of acute PE in our department: (a) patients who are short of breath (i.e., the majority of cases referred in this clinical contest), the scanning protocol is a high-pitch mode, obtained with single-energy CT; (b) when they can hold their breath for 4-6 seconds, the scanning mode is based on dual-energy CT.

On the basis of 10 segments per lung, 540 segments in Group 1 and 600 segments in Group 2 were included for lung perfusion analysis. Among the 1140 segments to-be-analyzed, 34 segments (2.98%) were excluded from the comparative analysis because of the impossibility to evaluate perfusion in areas of lung consolidation (i.e., lung infarction) or passive atelectasis in close contact to pleural effusion. The inter-technique comparison was thus undertaken at the level of 1106 segments (**Figure 2**).

3-Analyzed parameters

3-1: Characteristics of the study population

At a patient level, the following parameters were recorded: age, sex, weight and height enabling us to calculate the body mass index, smoking history and tobacco consumption. In Group 1, the distribution of clots, severity of arterial obstruction and presence of

features suggestive of right ventricular dysfunction were recorded. Acute pulmonary embolism was rated as uni- or bilateral, with clots exclusively located within subsegmental and/or segmental arteries (i.e. peripheral PE) or present within central (i.e., from the pulmonary trunk to lobar arteries) and/or peripheral pulmonary arteries. The clot burden of each patient was calculated using the Mastora scoring system (**32**). This scoring system is applied to five mediastinal (*the pulmonary artery trunk, the right and left main pulmonary arteries, and the right and left interlobar arteries*) , six lobar *(the right truncus anterior, the left upper lobe pulmonary artery (upper arterial branch, i.e., the culminal branch), the right middle lobe pulmonary artery, the left upper lobe pulmonary artery (the lower arterial branch, i.e., the lingular artery),and the right and left lower lobe pulmonary arteries)* and 20 segmental arteries *(the three right and left upper lobe (upper division) segmental arteries; the two right middle lobe and left upper lobe (lower division) segmental arteries; and the five right and left lower lobe segmental arteries).*The CT severity score is based on the percentage of the obstructed surface of each central and peripheral pulmonary arterial section using a 5-point scale: 1:<25%; 2:25-49%; 3:50-74%; 4:75-99%; 5: 100%. The maximum obstruction score is 155. The heart strain was evaluated on morphological basis, i.e., the right/left ventricular diameter ratio >1 with leftward displacement on the interventricular septum; when these features were present and seen in the absence of increased thickness of the right ventricular wall (i.e. the right ventricular wall thickness <4mm), this suggested acute right ventricular dysfunction in the context of acute PE.

3-2 : Quality of CT angiograms :

On each CT angiogram, measurements of attenuation value within the pulmonary trunk, the apical segmental artery of the right upper lobe (RA1) and the posterior segmental artery of the right lower lobe (RA10), the latter measurements enabling calculation of the gradient of attenuation between RA1 and RA10.

3-3: Perfusion imaging

- *Detection of perfusion defects*

The analysis was obtained at the level of analyzable segments; in each of these segments, the readers determined the number of PE-type defects (triangular, pleural-based) identified.

- *Subjective image quality evaluation*

Readers rated subjective image noise with a 3-point scale (score 3: marked noise, precluding perfusion analysis; score 2: moderate noise, and score 1: mild noise, both enabling perfusion analysis). They scored fissure visibility as follows: fissures not detected (score 3); fissures detectable but blurred (score 2) and fissures clearly identified as fine linear structures (score 1). They also rated the presence of artifacts at the level of ribs, diaphragmatic dome, around cardiac cavities and opacified systemic veins at the level of lung apices (i.e., around the subclavian artery) and around the superior vena cava, as marked (score 3), moderate (score 2) and mild (score 1); scores 1 and 2 did not alter the overall quality of perfusion images and score 3 precluded interpretation of perfusion in the vicinity of artifacts.

- *Subjective and objective evaluation of perfusion defects*

This analysis was undertaken at the level of one defect per segment, either the only one depicted or the largest defect in case of multiple defects. Borders of this defect were rated as well defined (score 1) or blurred (score 2). Measurement of attenuation values within the defect and in the adjacent well-perfused lung parenchyma was obtained; the ROIs for these measurements had the largest surface without crossing vascular or bronchial structures, in areas devoid of artifacts.

4-Conditions of image analysis

The reading of Lung PBV images (i.e. transverse CT sections and MPRs) was first undertaken to detect PE-type perfusion defects and rate subjective image quality. This

analysis required simultaneous display of Lung PBV reconstructions and corresponding lung images to ensure reliable location of defect(s) and to avoid misinterpretation of fissures for PE-related defects. A second reading session was obtained in similar conditions for the analysis of Lung Mono images. A third session focused on quantitative analysis of perfusion defects; it required simultaneous display of Lung PBV and Lung Mono images to ensure similar positioning of ROIs within perfused and non-perfused lung areas. The three reading sessions were obtained by consensus between two readers, i.e., a junior reader with 3 years of experience in CT (JP) and a senior reader with a 10-year experience (AH). They were unaware of the presence or absence of acute pulmonary embolism and read anonymized cases, presented in random order. Analysis of morphologic imaging was undertaken by a single reader (i.e., the junior reader).

5-Statistical analysis

This is an exploratory study aimed at providing preliminary results on a new reconstruction technique for dual-energy CT lung perfusion. No formal sample size calculation was performed. We planned to recruit 30 patients in each group, i.e., patients with and without PE. Data were analyzed using the SAS software version 9.4 (SAS Institute, Cary, NC). Quantitative variables are reported as mean (standard deviation), median (interquartile range) and range values and categorical variables are reported as numbers (percentage). Patients and CT angiogram characteristics are compared between patients with and without PE by using Mann-Whitney U tests for quantitative variables and by using the Chi-Square test (or Fisher's exact when excepted cell frequency<5) for categorical variables. In the overall study sample (patients with and without PE pooled together), we compared the perfusion image quality score according to the imaging techniques (Lung PBV vs Lung Mono) by using a Wilcoxon signed-rank test. We also used a Wilcoxon signed-rank test to compare the attenuation values between the two imaging techniques in patients with PE. Statistical testing was conducted at the two-tailed α-level of 0.05.

RESULTS

1-Study population

As shown in **Table 2**, there was no significant difference between Group 1 and Group 2 in the distribution of BMI (p=0.19), distribution of BMI categories (p=0.23), number of smokers (p=0.06); in Group 1, there was a trend toward a higher tobacco consumption without reaching statistical significance (p=0.057). Group 1 had a higher proportion of males (p=0.034) and patients were significantly older (p=0.028). The distribution, severity of PE and PE-related defects in Group 1 are summarized in **Table 3**.

2- Quality of CT angiograms

As shown in **Table 4**, there was no significant difference between Group 1 and Group 2 patients in the distribution of attenuation values within the pulmonary trunk (p=0.06), RA1 (p=0.056) and RA10 (p=0.17) nor in the distribution of differences in attenuation between RA1 and RA10 (p=0.13). The distribution of DLP did not differ between the two groups (p=0.23).

3- Detection of PE-type perfusion defects

At the level of the 1106 segments analyzed, there were concordant findings between Lung Mono and Lung PBV in 1104 segments (1104/1106; 99.8%) (absence of defects: n=968; presence of defects: n=138) (**Figure 3**) and discordant findings in 2 segments (RS4 and LS2 in two different Group 1 patients). These perfusion defects were confidently detected on Lung Mono images but not described on Lung PBV images. Combined analysis of Lung Mono and Lung PBV images suggested potential explanations for these discordant interpretations: (a) in LS2, the perfusion defect was likely to have been misinterpreted as cardiac motion artifact on Lung PBV images (**Figure 4**); (b) in RS4, the perfusion defect could have been missed because of marked image noise and a very coarse noise texture in this obese patient (**Figure 5**). Both patients had bilateral acute PE with multiple perfusion defects.

At a patient level, there were no PE-type perfusion defects detected on Lung Mono nor Lung PBV images in Group 2. The presence of emphysema in 9 patients (Group 1: n=5; Group 2: n=4), rated as mild in 5 patients (Group 1: n=2; Group 2: n=3) and moderate/ marked in 4 patients (Group 1: n=3; Group 2: n=1), did not interfere with PE-type perfusion defect analysis.

4- Subjective image quality of perfusion images

Overall study population (**Table 5**)

The distribution of scores of subjective noise significantly differed between Lung PBV and Lung Mono images ($p<0.0001$) with mild noise in 58.6% of Lung Mono images and no case of marked noise vs moderate and marked noise in 70.7% and 3.5% of Lung PBV images, respectively. The distribution of scores of fissure visibility significantly differed between Lung PBV and Lung Mono ($p<0.0001$) with fissures clearly identified in 77.6% of cases on Lung Mono images vs fissures rated as blurred (51.7%) or not detectable (48.3%) on Lung PBV images. There was no significant difference between the two categories of perfusion images regarding the distribution of scores of artifacts at the level of ribs, around the SVC and in the lung apex. However, the distribution of scores significantly differed at the level of the diaphragm ($p=0.0005$) and around cardiac cavities ($p=0.0039$) with a majority of Lung Mono images showing mild to moderate artifacts.

Study population stratified by BMI (**Table 6**)

The distribution of scores of image noise significantly differed between the two categories of perfusion images when considering the subgroups of underweight patients and patients with normal BMI as a whole ($p=0.0039$) and the subgroup of overweight patients ($p=0.0002$) but it did not differ for obese patients ($p=0.125$). On Lung Mono images, mild image noise was observed in 86.4% of underweight and normal BMI patients, in 50% of overweight patients and in 28.6% of obese patients (vs 54.5%, 9.1%

and 7.1% on Lung PBV images, respectively). In obese patients, marked image noise was not observed on Lung Mono images (vs 14.3% on Lung PBV images).

The distribution of scores of fissure visualization significantly differed between the two categories of perfusion images for underweight/normal BMI patients ($p<0.0001$), overweight ($p=0.016$) and obese ($p<0.0001$) patients. Fissures were rated as clearly identified on Lung Mono images in 95.5%, 77.3% and 50% of patients in underweight/normal BMI, overweight and obese patients respectively (versus 0% in the same categories on Lung PBV images). In obese patients, fissures were detected in all but one patient on Lung Mono images whereas they were rated as not detected in 92.9% of patients on Lung PBV images. **Figures 3, 4 and 5** illustrate image quality in different BMI categories.

5-Subjective and objective evaluation of perfusion defects

This evaluation was undertaken at the level of the 138 perfusion defects similarly depicted by both techniques.

On Lung Mono images, 29 defects had sharp borders (29/138; 21.01 %) and 109 (109/138; 78.99%) had blurred borders. On Lung PBV images, 18 defects (18/138; 13.04%) had sharp borders and 120 defects (86.96 %) had blurred borders.

The rating of defect borders was concordant between the two techniques in 90.6% of cases (125/138) and discordant in 9.4% (13/138). The 13 discordant ratings were observed as follows: (a) 12 defects were rated with well-defined borders (score 1) on Lung Mono images and rated as blurred (score 2) on Lung PBV images; (b) 1 defect was rated with well-defined borders on Lung PBV images (score 1) and with blurred borders on Lung Mono images (score 2). As shown in **Table 7**, the distribution of attenuation values within perfused lung and within defects were both significantly higher on Lung Mono images ($p<0.0001$). The distribution of gradient of attenuation between perfused areas and defects was significantly higher on Lung Mono images (median=73.5 HU; Q1=65.0; Q3=86.0) compared to Lung PBV (median=24.5 U; Q1=22.0; Q3=30.0) ($p<0.0001$). Similar trends were observed when stratifying the population of 28 patients

with PE according to their BMI (**Table 8**); because of the small number of individuals in the BMI categories, no statistical analysis could be performed.

DISCUSSION

To our knowledge, this is the first study investigating a new approach aimed at optimizing DECT lung perfusion imaging. Considering lung PBV imaging as the reference standard, our study was built as a two-step investigation, undertaken in the clinical context of acute pulmonary embolism known to be responsible for specific perfusion defects. The first step focused on the rate of detection of PE-type perfusion defects, considering that the image quality of Lung Mono images would be worth analyzing only if this new technique did not miss information accessible on reference images. Comparison between Lung Mono and Lung PBV images showed an almost perfect agreement, with concordant findings in all but 2 segments (i.e., rate of concordance of 99.8%). In the two discordant ratings, segmental perfusion defects were clearly depicted on Lung Mono images but not described on Lung PBV images. The most likely explanation was that they had been missed because of marked coarse image noise in an obese patient and misinterpreted as motion artifact in the second patient. This finding suggests an applicability for DECT whatever the patient body habitus, thus more widely applicable than Lung PBV.

The second step of our study was to evaluate whether the theoretical superiority of image quality on subtracted images was perceptible on images acquired in real-life conditions. The most striking finding was the higher spatial resolution of Lung Mono images. Fissures were clearly identified in 77.6% of cases on Lung Mono images while rated as blurred (51.7%) or not detectable (48.3%) on the majority of Lung PBV images. Detection of fissures is a key component for confident localization of perfusion abnormalities, especially in the context of peripheral chronic thromboembolic disease. While the objective image noise as measured in a CATPHAN 500 was higher for Lung Mono than Lung PBV, the noise texture was less patchy, coarse and grainy. This leads to a lower level of perceived subjective image noise on Lung Mono images which

participated in the overall impression of improved image quality. The distribution of scores of subjective noise significantly differed between the two techniques with mild image noise in the majority of Lung Mono images and no case of marked noise, while noise was rated as moderate and marked in 70.7% and 3.5% of Lung PBV images, respectively. Subjective improvement in image quality was logically perceptible in underweight patients and in patients with normal BMI. However, it was important to underline that subjective image quality was also more favorably rated on Lung Mono images in overweight and obese patients. In the latter category of patients, image noise was never rated as marked (vs 14.3% on Lung PBV images where it hampered perfusion analysis) and fissures were clearly identified in 50% of examinations while not detectable in 92.9% of Lung PBV images. On Lung Mono images, we also observed less pronounced artifacts at the level of the diaphragm and around cardiac cavities compared to Lung PBV, both contributing to the overall improvement in image quality.

A significantly higher gradient of attenuation between hypo- and normally perfused lung was demonstrated on Lung Mono images. This mainly resulted from the increased iodine signal at the level of the normally perfused lung parenchyma on subtracted monoenergetic images. In the Lung Mono approach, a 190 keV image (with negligible iodine contrast) is subtracted from a 40 keV image (with very high iodine contrast), subsequently generating an image with the CT numbers of iodine at 40 keV. On the Lung PBV image, the CT numbers of iodine correspond to an image acquired at 120 kV, with a mean energy of about 70 keV. Keeping in mind that the “background” without iodine (i.e., perfusion defects) has similar CT numbers both for lung PBV and for Lung Mono, the gradient of attenuation between perfused areas and defects is therefore much larger for Lung Mono than for lung PBV.

It was also interesting to note a significantly higher attenuation within the areas devoid of perfusion on LungMono images, suggesting that a subtle residual perfusion beyond the endoluminal clots or via a systemic collateral supply was detectable in patients with acute PE. However, this higher gradient of attenuation has no impact on the rating of the sharpness of defect borders with concordant findings on Lung Mono and

Lung PBV images in 90.6% of cases. The combination of increased iodine signal and lower image noise on Lung Mono images should open new horizons for lung perfusion in clinical practice. In COPD, one might expect detection of subtle changes within lung microcirculation, preceeding the depiction of morphologic changes (**33**). Among interstitial lung diseases, there are disorders with pulmonary vasculopathy that can develop in the absence of interstitial lung disease, as observed in systemic sclerosis (**34**). Their depiction at an early stage of the disease would be clinically helpful. In the specific context of acute pulmonary embolism, perfusion defects have already been shown to be useful for assessment of the clinical severity of PE and proposed to be used as an indicator of right ventricular dysfunction (**35,36**). In the population of patients suspected of PE but without evident thromboembolic clot on CTA, Taks et al have more recently reported that the volume of perfusion defects appeared to be predictive for all-cause mortality (**37**). An improved quality of perfusion imaging could also benefit the recognition of distal obstruction of the pulmonary arteries in peripheral CTEPH (**19,38**) and facilitate the depiction of lung microcirculation alterations in pulmonary arterial hypertension (**17**) as well as in those observed during the acute phase and in the follow-up of COVID-19 pneumonia (**29**). Lastly, in more technically-oriented considerations, Lung Mono imaging could be an interesting option for an improved reliability of CT-based measurements of iodine concentration (**24,39**).

This study suffers from several limitations that have to be acknowledged. First, this study investigated lung perfusion imaging in a single clinical setting, namely acute pulmonary embolism, whereas image quality could have been tested in other diseases with perfusion alterations. In the absence of external gold standard for assessment of perfusion defects, we limited the diagnostic accuracy of perfusion images to the depiction of PE-type defects, known to be easily recognized by their shape and location. We considered that missing PE-type defects would disqualify Lung Mono images from further qualitative evaluation. Second, our study population was limited to 58 patients. This resulted from the strict inclusion criteria, avoiding patients with respiratory co-morbidities and patients with nonobstructive endoluminal clots that did not alter lung

perfusion. Moreover, dual-energy CT is not the favored scanning mode for dyspneic patients suspected of acute PE in routine clinical practice, preferably scanned with single-energy, high-pitch acquisitions to ensure motion artifact-free examinations. Third, perfusion analysis was performed by consensus between two readers without calculation of intra- and inter-reader agreement. However, the two readers analyzed anonymized cases, read in random order and without knowledge of the presence or absence of acute PE. Lastly, one should mention the longer time needed to generate Lung Mono images compared to Lung PBV (i.e., in the range of 3-4 minutes), not because of a longer time for postprocessing but because of the need to transfer monoenergetic images to the prototype reconstruction tool.

In conclusion, this is the first study demonstrating the improved quality of subtracted monoenergetic perfusion imaging over traditional Lung PBV imaging in a clinically representative study population of patients with suspected PE.

REFERENCES

1-Albrecht MH, Vogl TJ, Martin SS, et al. Review of clinical applications for virtual monoenergetic dual-energy CT. Radiology 2019; 293: 260-71

2-Thieme SF, Johnson TR, Lee C, et al. Dual-energy CT for the assessment of contrast material distribution in the pulmonary parenchyma. Am J Roentgenol 2009; 193: 144-9

3-Geyer LL, Scherr M, Körner M, et al. Imaging of acute pulmonary embolism using a dual energy CT system with rapid kVp switching: initial results. Eur J Radiol 2012; 81: 3711-18

4-Bauer RW, Kramer S, Renker M, et al. Dose and image quality at CT pulmonary angiography: comparison of first and second generation dual-energy CT and 64-slice CT. Eur Radiol 2011; 21: 2139-47

5-Schenzle JC, Sommer WH, Neumaier K, et al. Dual energy CT of the chest: how about the dose? Invest Radiol 2010; 45: 347-53

6-Mettler FA Jr, Huda W, Yoshizumi TT, et al. Effective doses in radiology and diagnostic nuclear medicine: a catalog. Radiology 2008; 248: 254-63

7-Lenga L, Trapp F, Albrecht MH, et al. Single- and dual-energy CT pulmonary angiography using second- and third-generation dual-source CT systems: comparison of radiation dose and image quality. Eur Radiol 2019; 29: 4603-12

8-Thieme SF, Becker CR, Hacker M, K et al. Dual energy CT for the assessment of lung perfusion-correlation to scintigraphy. Eur J Radiol 2008 ; 68 : 369-374

9-Thieme SF, Graute V, Nikolaou K, et al. Dual-energy CT lung perfusion imaging: correlation with SPECT/CT. Eur J Radiol 2012; 81: 360-5

10-Fuld MK, Halaweish AF, Haynes SE, Divekar AA, Guo J, Hoffman EA. Pulmonary perfused blood volume with dual-energy CT as surrogate for pulmonary perfusion assessed with dynamic multidetector CT. Radiology 2013;267:747-56.

11-Tang CX, Yang GF, Schoepf UJ, Han ZH, Qi L, Zhao YE, Wu J, Zhou CS, Zhu H, Stubenrauch AC, Mangold S, Zhang LJ, Lu GM. Chronic thromboembolic pulmonary

hypertension: Comparison of dual-energy computed tomography and single photon emission computed tomography in canines. Eur J Radiol. 2016;85:498-506
12-Pontana F, Faivre JB, Remy-Jardin M, et al. Lung perfusion with dual-energy multidetector-row CT (MDCT): feasibility for the evaluation of acute pulmonary embolism in 117 consecutive patients. Acad Radiol 2008; 15: 1494-1504
13-Im DJ, Hur J, Han K, Suh YJ, Hong YJ, Lee HJ, Kim YJ, Choi BW. Prognostic Value of Dual-Energy CT-Based Iodine Quantification versus Conventional CT in Acute Pulmonary Embolism: A Propensity-Match Analysis. Korean J Radiol. 2020;21:1095-1103
14-Renard B, Remy-Jardin M, Santangelo T et al. Dual-energy CT angiography of chronic thromboembolic disease: can it help recognize links between the severity of pulmonary arterial obstruction and perfusion defects? Eur J Radiol 2011; 79: 467-472
15-Nakazawa T, Watanabe Y, Hori Y et al. Lung perfused blood volume images with dual-energy computed tomography for chronic thromboembolic pulmonary hypertension: correlation to scintigraphy with single-photon emission computed tomography. J Comput Assist Tomogr 2011; 35: 590-595
16-Saeedan MB, Bullen J, Heresi GA et al. Morphologic and Functional Dual-Energy CT Parameters in Patients With Chronic Thromboembolic Pulmonary Hypertension and Chronic Thromboembolic Disease. AJR Am J Roentgenol. 2020;215:1335-1341.
17-Giordano J, Khung S, Duhamel A et al. Lung perfusion characteristics in pulmonary arterial hypertension (PAH) and peripheral forms of chronic thromboembolic pulmonary hypertension (pCTEPH): dual-energy CT experience in 31 patients. Eur Radiol 2017; 27: 1631-1639
18-Renapurkar RD, Bolen MA, Shrikanthan S, Bullen J, Karim W, Primak A, Heresi GA. Comparative assessment of qualitative and quantitative perfusion with dual-energy CT and planar and SPECT-CT V/Q scanning in patients with chronic thromboembolic pulmonary hypertension. Cardiovasc Diagn Ther. 2018;8: 414-422
19-Le Faivre J, Duhamel A, Khung S et al. Impact of CT perfusion imaging on the assessment of peripheral chronic pulmonary thromboembolism: clinical experience in 62 patients. Eur Radiol. 2016;26:4011-4020

20-Dournes G, Verdier D, Montaudon M et al. Perfusion and angiography in chronic thromboembolic pulmonary hypertension: diagnostic accuracy and concordance with radionuclide scintigraphy. Eur Radiol 2014 ; 24 : 42-51
21-Masy M, Giordano J, Petyt G, et al. Dual-energy CT (DECT) lung perfusion in pulmonary hypertension: concordance rate with V/Q scintigraphy in diagnosing chronic thromboembolic pulmonary hypertension (CTEPH). Eur Radiol 2018; 12: 5100-5120
22- Pansini V, Remy-Jardin M, Faivre JB et al. Assessment of lobar perfusion in smokers according to the presence and severity of emphysema: preliminary experience with dual-energy CT angiography. Eur Radiol. 2009;19:2834-43.
23- Iyer KS, Newell JD Jr, Jin D et al. Quantitative Dual-Energy Computed Tomography Supports a Vascular Etiology of Smoking-induced Inflammatory Lung Disease. Am J Respir Crit Care Med. 2016;193:652-61.
24-Moon JW, Bae JP, Lee HY, et al. Perfusion- and pattern-based quantitative CT indexes using contrast-enhanced dual-energy computed tomography in diffuse interstitial lung disease: relationships with physiologic impairment and prediction of prognosis. Eur Radiol 2016; 26: 1368-77
25-Si-Mohamed S, Moreau-Triby C, Tylski P et al. Head-to-head comparison of lung perfusion with dual-energy CT and SPECT-CT. Diagn Interven Imaging 2020; 101: 299-310
26-Lang M, Som A, Mendoza DP, Flores EJ, Reid N, Carey D, Li MD, Witkin A, Rodriguez-Lopez JM, Shepard JO, Little BP. Hypoxaemia related to COVID-19: vascular and perfusion abnormalities on dual-energy CT. Lancet Infect Dis. 2020;20:1365-1366
27-Ganti S, Kok SSX, Aftab S et al. Spectrum of lung perfusion changes on dual-energy CT in COVID-19: incremental benefit to conventional CT. Emerg Radiol. 2021; 8:1-5.
28-Grillet F, Busse-Coté A, Calame P et al. COVID-19 pneumonia: microvascular disease revealed on pulmonary dual-energy computed tomography angiography. Quant Imaging Med Surg. 2020;10:1852-1862.

29-Remy-Jardin M, Duthoit L, Perez T et al. Assessment of pulmonary arterial circulation 3 months after severe SARS-CoV-2 pneumonia: dual-energy CT (DECT) angiographic study in 55 patients. EClinMed 2021 (in press)
30- Johnson TR, Krauss B, Sedlmair M et al. Material differentiation by dual energy CT: initial experience.
Eur Radiol. 2007;17:1510-7
31-Grant KL, Flohr T, Krauss B et al. Assessment of an advanced image-based technique to calculate virtual monoenergetic computed tomographic images from a dual-energy examination to improve contrast-to-noise ratio in examinations using iodinated contrast media. Invest Radiol 2014; 49: 586-592
32- Mastora I, Remy-Jardin M, Masson P et al. Severity of acute pulmonary embolism: evaluation of a new spiral CT angiographic score in correlation with echocardiographic data. Eur Radiol 2003; 13: 29-35
33-Young AL, Bragman FJS, Rangelov B et al. Disease progression modeling in Chronic Obstructive Pulmonary Disease. Am J Respir Crit Care Med 2020; 201: 294-302
34-Launay D, Sobanski V, Hachulla E, Humbert M. Pulmonary hypertension in systemic sclerosis: different phenotypes. Eur Respir J 2017; 26: 170056
35-Bauer RW, Dual-energy pulmonary blood volume assessment in acute PE: correlation with D-dimer level, right heart strain and clinical outcome. Eur Radiol 2011; 21: 1914-1921
36-Sakamoto A, Sakamoto I, Nagayama H et al. Quantitative lung perfusion blood volume with dual-energy CT: assessment of the severity of acute pulmonary embolism. AJR 2014; 203: 287-291
37-Takx RAP, Henzler T, Schoepf UJ et al. Predictive value of perfusion defects on dual-energy CTA in the absence of thromboembolic clots. J Cardiovasc Comput Tomogr 2017; 11: 183-187
38-Lysdahlgaard S, Hess S, Gerke O, Kusk MW. A systematic literature review and meta-analysis of spectral CT compared to scintigraphy in the diagnosis of acute and chronic pulmonary embolisms. Eur Radiol 2020; 30: 3624-33

39-Euler A, Solomon J, Mazurowski MA, et al. How accurate and precise are CT based measurements of iodine concentration? A comparison of the minimum detectable concentration difference among single source and dual source dual energy CT in a phantom study. Eur Radiol 2019; 29: 2069-78

FIGURE CAPTIONS

Figure 1: Objective assessment of image quality in terms of noise (standard deviation in circular region of interest) and resolution (line pair per centimeter high resolution test bar pattern) using CAT phantom insert CTP528 (Catphan 500, The Phantom Laboratory, USA).

Figure 1a corresponds to the morphologic image generated from both tubes, often described as the averaged image, assimilated to a traditional 120 kV image.

Figure 1b corresponds to the perfusion image reconstructed by three-compartment decomposition using the Lung PBV algorithm.

Figure 1c corresponds to the perfusion image generated by subtraction of virtual monoenergetic images.

The Lung Mono algorithm (**Fig 1c**) maintains resolution of averaged morphologic images (**Fig 1a**) (6 lp/cm), whereas the Lung PBV resulted in a lower resolution (4 lp/cm) (**Fig 1b**). The highest visible resolution pattern for all three setups are highlighted in yellow. Noise was 11.2 HU and 19.4 HU for the Lung PBV and the Lung Mono, respectively. The subjective noise texture is more patchy and grainy for the Lung PBV images than for the Lung Mono images.

Figure 2: Study flowchart

Figure 3: Dual-energy CT angiographic examination obtained in a 62-year-old overweight female with acute pulmonary embolism (160 cm; 70 kg; BMI: 27.34 $kg.cm^2$)

Paired Lung Mono (**Figure 3a**) and Lung PBV (**Figure 3b**) images obtained at the level of the right bronchus intermedius. Paired Lung Mono (**Figure 3c**) and Lung PBV (**Figure 3d**) images obtained at the level of the inferior pulmonary veins.

Similar depiction of triangular, peripheral perfusion defects in the right middle (double white arrows) and right lower (single white arrows) lobes.
In Lung Mono images (**Figures 3a, 3c**), clear identification of the right and left major fissures as fine linear opacities, not detectable on Lung PBV images (**Figures 3b, 3d**). The right minor fissure is visible but blurred on the Lung Mono image (white arrowheads, **Figure 3a**); it appears as a large zone of hypoattenuation on the Lung PBV image (white arrowheads, **Figure 3b**).

Figure 4: Dual-energy CT angiographic examination obtained in a 72-year-old male with acute pulmonary embolism in a context of bronchopulmonary carcinoma. Overweight patient (185 cm; 95 kg; BMI: 27.75 $kg.cm^2$).
Paired Lung Mono (**Figure 4a**) and Lung PBV (**Figure 4b**) images obtained at the level of the right bronchus intermedius. **Figure 4c:** mediastinal image at the level of the anterior segmental artery of the left upper lobe (LA2).

The small arrows in **Figures 4a** and **4b** point to a large perfusion defect in the anterior segment of the left upper lobe that was depicted in the Lung Mono image and misinterpreted as motion artifact in the Lung PBV image. This perfusion defect was linked to the presence of an obstructive clot within LA2 (arrows; **Figure 4c**).
Similar depiction of defects in the right upper lobe (large arrow) and in the apical segment of the right lower lobe (arrowhead) in **Figures 4a** and **4b**.

Figure 5: Dual-energy CT angiographic examination obtained in a 61-year-old female with acute pulmonary embolism. Patient with morbid obesity (160 cm; 120 kg; BMI: 46.8 $kg.cm^2$).
Large perfusion defect due to peripheral acute PE in the lateral segment of the right middle lobe (arrows **in Figures 5a, 5b**). Less image noise and improved spatial resolution are observed in **Figure 5a**. Similar ratings of artifacts around cardiac cavities (small stars) and in the paravertebral regions (large stars).

Table 1
Scanning protocol and reconstruction parameters

Acquisition parameters	
Tube A	70 kV-402 mAs (<65 kg) 80 kV-207 mAs (65-80 kg) 90 kV-208 mAs (>80 kg)
Tube B	Sn 150 kV-115 mAs
Collimation	64 x 0.6 mm x 2
Pitch	0.55
Rotation time*, s*	0.25
Care Dose 4D	off
Caudo-cranial acquisitions	+
End-inspiratory acquisition	+
Injection parameters	
Iodine concentration, *mg I/mL*	400
Flow rate*, mL/s*	4
Volume administered, *mL*	60 *(iodine)* + 40 *(diluted contrast medium)*
ROI position	ascending aorta
Threshold, *HU*	100
Reconstruction parameters	
Lung images: -thickness, *mm* -intervals, *mm* -kernel	 1 1 Bl57
Mediastinal images: -thickness, *mm* -intervals, mm -kernel	 1 1 Br36
Perfusion images: -thickness, *mm* -intervals, *mm* -range of HU selected -range user -kernel	 1 1 -1000 HU/-200 HU 2 Q40

Table 2

	Group 1 **Presence of PE** n=28	**Group 2** **Absence of PE** n=30	**P**
Sex ratio (males/females), n (%)	19 (67.9) ; 9 (32.1)	12 (40.0) ; 18 (60.0)	0.034 *
Age, yr mean ± SD median (Q1; Q3) range (minimum; maximum)	 57.2 ± 14.0 56.5 (48.0 ; 68.5) 28.0 | 83.0	 47.4 ± 17.1 42.0 (33.0 ; 64.0) 24.0 | 76.0	 0.028***
BMI, kg/m^2 mean ± SD median (Q1; Q3) range (minimum ; maximum)	 27.9 ± 5.6 27.6 (24.3 ; 29.9) 19.3 | 46.9	 26.4 ± 6.6 25.8 (21.5 ; 30.4) 17.1 | 44.1	 0.19***
BMI categories underweight *(<18 kg/m^2)*, n (%) normal *(18-25 kg/m^2)*, n (%) overweight *(25-29 kg/m^2)*, n (%) obese *(≥30 kg/m^2)*, n (%)	 0 (0.0) 8 (26.7) 14 (50.0) 6 (21.4)	 1 (3.3) 13 (43.3) 8 (26.7) 8 (26.7)	 0.23**
Smokers, n (%)	16 (57.1%)	10 (33.3%)	0.068*
Tobacco consumption, pack-year mean ± SD median (Q1; Q3) range (minimum ; maximum)	 19.4 ± 17.9 15.0 (5.5 ; 27.5) 1.0 | 60.0	 6.9 ± 7.2 3.5 (2.0 ; 15.0) 1.0 | 20.0	 0.057***

NB: comparisons were obtained with the chi^2 test (*), Fisher's exact test (**) and Mann-Whitney U test (***).
Abbreviations: SD: standard deviation; BMI: body mass index; Q1: first quartile; Q3: third quartile

Table 3

Distribution, severity of PE and PE-related perfusion defects in Group 1

Distribution of acute PE	
Type of PE: -unilateral, n (%) -bilateral, n (%)	 8 (28.6%) 20 (71.4%)
Location of clots -exclusively within central PAs -exclusively within peripheral PAs, n (%) -within central & peripheral PAs, n (%)	 0 12 (42.9%) 16 (57.1%)
Severity of acute PE	
CT obstruction score, % mean (SD) median range	 22.7 (16.3) 21.3 3.2 – 56.8
Heart strain RV/LV ratio >1, n (%)	 3 (10.7%)
PE-related perfusion defects	
Number of PE-type perfusion defects per patient mean (SD) median range	 4.9 (2.7) 5 1-9
Extent of PE-type perfusion defects -patients with segmental & subsegmental defects, n -patients with only subsegmental defects, n -patients with only segmental defects, n	 18 9 1

NB: Central pulmonary arteries include main, lobar and interlobar pulmonary arteries; peripheral pulmonary arteries include segmental and subsegmental pulmonary arteries.

Abbreviations: PE: pulmonary embolism; PA: pulmonary artery; RV: right ventricle; LV: left ventricle; SD: stabdard deviation

Table 4

Characteristics of CT angiograms in Group 1 and Group 2

	Group 1 **Presence of PE** 28 patients	**Group 2** **Absence of PE** 30 patients	**P**
Attenuation within the pulmonary trunk, HU mean ± SD median (Q1; Q3) range (minimum; maximum)	 351.5 ± 132.9 311.5 (264.5 ; 387.0) 184.0 | 704.0	 439.8 ± 185.0 434.5 (284.0 ; 534.0) 183.0 | 852.0	0.060
Attenuation within RA1, HU mean ± SD median (Q1; Q3) range (minimum; maximum)	401.6 ± 146.4 374.0 (307.5 ; 440.5) 208.0 | 833.0	488.6 ± 189.6 493.5 (348.0 ; 597.0) 213.0 | 935.0	0.056
Attenuation within RA10, HU mean ± SD median (Q1; Q3) range (minimum; maximum)	415.1 ± 144.4 370.0 (307.0 ; 492.5) 199.0 | 805.0	471.7 ± 163.7 432.5 (365.0 ; 552.0) 215.0 | 885.0	0.17
Delta between RA10 and RA1, HU mean ± SD median (Q1; Q3) range (minimum; maximum)	54.9 ± 31.7 53.5 (29.0; 72.5) 4 | 149	42.8 ± 31.5 37.0 (21.0; 65.0) 0 | 137	0.13
Dose-Length-Product, mGy.cm mean ± SD median (Q1; Q3) range (minimum; maximum)	308.4 ± 63.4 282.5 (262.5 ; 352.5) 241.0 | 436.0	314.7 ± 54.1 297.5 (277.0; 336.0) 231.0 | 434.0	0.23

NB: comparisons were obtained with the Mann-Whitney U test
Abbreviations: RA1: anterior segmental artery of the right upper lobe; RA10: posterior segmental artery of the right lower lobe; HU: Hounsfield unit; SD: standard deviation: Q1: first quartile; Q3: third quartile; mGy.cm: milligray.centimeter

Table 5
Comparison of lung perfusion image quality in the study population

	Lung PBV 58 examinations	**Lung Mono** 58 examinations	**P**
Subjective noise, HU mild (score 1), n (%) moderate (score 2), n (%) marked (score 3), n (%)	 15 (25.9) 41 (70.7) 2 (3.5)	 34 (58.6) 24 (41.4) 0 (0.0)	 <0.0001
Fissure visibility clearly identified (score 1), n (%) visible but blurred (score 2), n (%) not detected (score 3), n (%)	 0 (0) 30 (51.7) 28 (48.3)	 45 (77.6) 12 (20.7) 1 (1.7)	 <0.0001
Artifacts at the level of ribs mild (score 1), n (%) moderate (score 2), n (%) marked (score 3), n (%)	 30 (51.7) 28 (48.3) 0 (0)	 32 (55.2) 26 (44.8) 0 (0)	 0.6250
Artifacts at the level of the diaphragm mild (score 1), n (%) moderate (score 2), n (%) marked (score 3), n (%)	 20 (34.5) 34 (58.6) 4 (6.9)	 30 (51.7) 26 (44.8) 2 (3.4)	 0.0005
Artifacts at the level of lung apex mild (score 1), n (%) moderate (score 2), n (%) marked (score 3), n (%)	 12 (20.7) 37 (63.8) 9 (15.5)	 12 (20.7) 38 (65.5) 8 (13.8)	 1.0000
Artifacts around the SVC mild (score 1), n (%) moderate (score 2), n (%) marked (score 3), n (%)	 16 (27.6) 39 (67.2) 3 (5.2)	 17 (29.3) 38 (65.5) 3 (5.2)	 1.0000
Artifacts around the cardiac cavities mild (score 1), n (%) moderate (score 2), n (%) marked (score 3), n (%)	 1 (1.7) 45 (77.6) 12 (20.7)	 3 (5.2) 50 (86.2) 5 (8.6)	 0.0039

NB: comparisons were obtained with the Wilcoxon signed-rank test
Abbreviations: SVC: superior vena cava; HU: Hounsfield unit.

Table 6
Comparison of quality of perfusion imaging according to patient BMI

IMAGE NOISE	**Rating of subjective noise on Lung PBV images**	**Rating of subjective noise on Lung Mono images**	**P**
Patients with normal BMI and underweight patients (n=22)			
mild noise (score 1), n (%) moderate noise (score 2), n (%) marked noise (score 3), n (%)	12 (54.5%) 10 (45.6%) 0 (0%)	19 (86.4%) 3 (13.6%) 0 (0%)	0.0039
Overweight patients (n=22)			
mild noise (score 1), n (%) moderate noise (score 2), n (%) marked noise (score 3), n (%)	2 (9.1%) 20 (90.9%) 0 (0%)	11 (50.0%) 11 (50.0%) 0 (0%)	0.0002
Obese patients (n=14)			
mild noise (score 1), n (%) moderate noise (score 2), n (%) marked noise (score 3), n (%)	1 (7.1%) 11 (78.6%) 2 (14.3%)	4 (28.6%) 10 (71.4%) 0 (0%)	0.125

FISSURE VISUALIZATION	**Rating of fissure visualization on Lung PBV images**	**Rating of fissure visualization on Lung Mono images**	**p**
Patients with normal BMI and underweight patients (n=22)			
Clearly identified (score 1), n (%) Visible but blurred (score 2), n (%) Not detected (score 3), n (%)	0 (0%) 17 (77.3%) 5 (22.7%)	21 (95.5%) 1 (4.5%) 0 (0%)	<0.0001
Overweight patients (n=22)			
Clearly identified (score 1), n (%) Visible but blurred (score 2), n (%) Not detected (score 3), n (%)	0 (0%) 12 (54.5%) 10 (45.5%)	17 (77.3%) 5 (22.7%) 0 (0%)	0.016
Obese patients (n=14)			
Clearly identified (score 1), n (%) Visible but blurred (score 2), n (%) Not detected (score 3), n (%)	0 1 (7.1%) 13 (92.9%)	7 (50.0%) 6 (42.9%) 1 (7.1%)	<0.0001

NB: Comparisons were obtained with the Wilcoxon signed-rank test.

Table 7
Comparison of attenuation values within perfused and non-perfused areas between Lung PBV and Lung Mono images in the 28 examinations with PE-perfusion defects.

	Lung PBV	**Lung Mono**	**P**
Attenuation within perfusion defect, HU mean ± SD median (Q1; Q3) range (minimum; maximum)	 3.5 ± 2.2 3.0 (2.0 ; 4.5) 1.0 | 9.0	 11.4 ± 6.1 10.5 (6.5 ; 16.5) 1.0 | 26.0	 <0.0001
Attenuation within perfused lung, HU mean ± SD median (Q1; Q3) range (minimum; maximum)	 30.4 ± 9.2 26.5 (24.0 ; 33.5) 15.0 | 55.0	 89.1 ± 19.9 85.0 (74.0 ; 100.0) 50.0 | 131.0	 <0.0001
Delta of attenuation between perfused and non-perfused lung mean ± SD median (Q1; Q3) range (minimum; maximum)	 26.9 ± 8.4 24.5 (22.0 ; 30.0) 12.0 | 46.0	 77.7 ± 20.0 73.5 (65.0 ; 86.0) 40.0 | 121.0	 <0.0001

NB: comparisons were obtained with the Wilcoxon signed-rank test.
Abbreviations: SD: standard deviation; HU: Hounsfield unit; Q1: first quartile; Q3: third quartile

Table 8
Comparison of attenuation values within perfused and non-perfused areas between Lung PBV and Mung Mono images according to the patient BMI

	Delta of attenuation between perfused and non-perfused areas on Lung PBV images	Delta of attenuation between perfused and non-perfused areas on Lung Mono images
Patients with normal and underweight BMI (< 25) (n=8)		
mean ± SD median (Q1; Q3) range (minimum; maximum)	31.4 ± 9.6 28.5 (24.0; 40.0) 20.0 i 46.0	85.9 ± 24.4 75.5 (69.0; 110.5) 56.0 I 121.0
Overweight patients (n=14)		
mean ± SD median (Q1; Q3) range (minimum; maximum)	25.6 ± 7.8 23.0 (21.0; 29.0) 17.0 I 44.0	73.1 ± 17.1 65.5 (64.0; 79.0) 53.0 I 116.0
Obese patients (n=6)		
mean ± SD median (Q1; Q3) range (minimum; maximum)	23.8 ± 6.6 25.5 (22.0 – 28.0) 12.0 I 30.0	77.3 ± 20.1 82.0 (74.0; 87.0) 40.0 I 99.0

Abbreviations: SD: standard deviation; HU: Hounsfield unit; Q1: first quartile; Q3: third quartile; BMI: body mass index

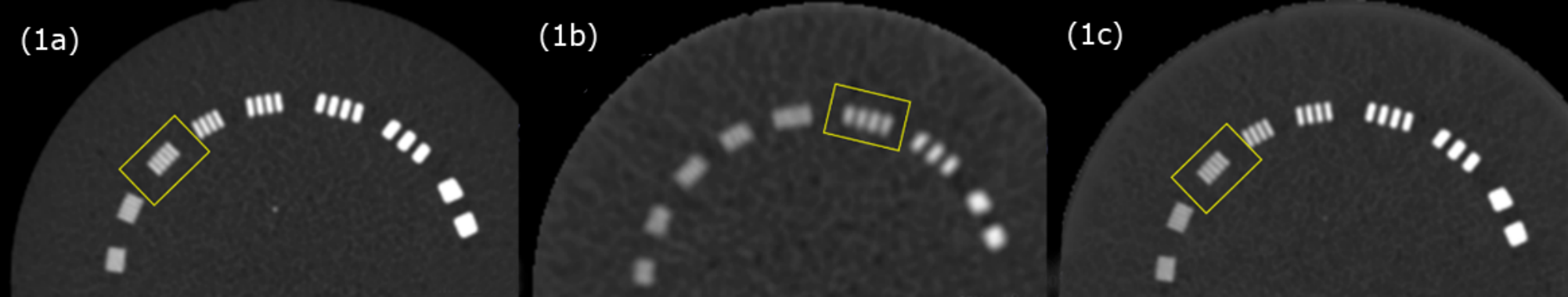
(1a)
(1b)
(1c)

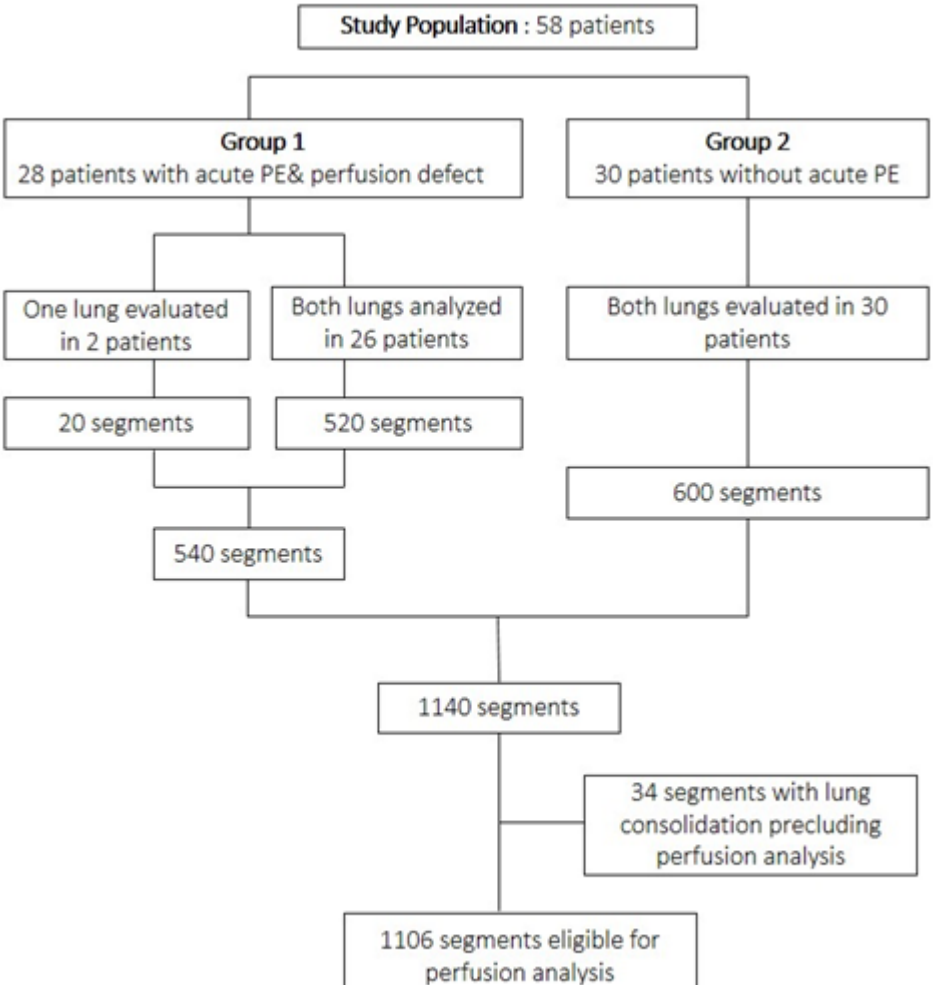
Study Population : 58 patients
Group 1
28 patients with acute PE& perfusion defect
Group 2
30 patients without acute PE
One lung evaluated in 2 patients
Both lungs analyzed in 26 patients
Both lungs evaluated in 30 patients
20 segments
520 segments
600 segments
540 segments
1140 segments
34 segments with lung consolidation precluding perfusion analysis
1106 segments eligible for perfusion analysis